Calculation Methods for Electromagnetically Excited Noise in Induction Motors

M. Al Nahlaoui, D. Braunisch, B. Eichinger, S. Kulig, B. Ponick, U. Werner

***Abstract*— The development of low-noise motors will help to protect the environment and result in a competitive advantage. Designing low-noise electric motors means that it is necessary to predict the noise characteristics of the electric motor in the early conceptual phase. Customizing means that it is necessary to be able to estimate how the modifications affect the noise behavior of the motor. This paper presents two methods to calculate the electromagnetically excited noise of an electric motor, a numerical method for a more accurate result in the design process, and an analytical method for fast estimation in the customizing process.**

***Index Terms*— Analytical models, Finite element methods, Induction motors, Magnetic noise, Modal analysis**

I. INTRODUCTION

THE noise sources of an electric motor can be divided into two fields: mechanical origin and electromagnetic origin. Especially for inverter-fed motors with variable speed, the noise of electromagnetic origin is of special interest. For this reason a project with two universities was set up to develop an analytical and a numerical method for calculating the electromagnetically excited noise.

Focus of the numerical method is the calculation of radial force waves coming from the electromagnetic field. In combination with a response analysis and a noise radiation calculation, this should give a precise forecast of the noise radiation. For the analytical method, the calculation of the electromagnetic, radial force wave already exists but the vibration is calculated with a simple ring. Here, it is necessary to describe the mechanical system in more detail to take into consideration the different housing geometries.

Manuscript received June 1, 2011.

Masen Al Nahlaoui; TU Dortmund University, Institute of Electrical Drives and Mechatronics; Emil-Figge-Str. 70; 44227 Dortmund (masen.nahlaoui@tu-dortmund.de)

Dirk Braunisch; Leibniz Universität Hannover, Institute for Drive Systems and Power Electronics; Welfengarten 1; 30167 Hanover, Germany (Braunisch@ial.uni-hannover.de)

Benjamin Eichinger; Siemens AG, Industry Sector, Drive Technologies Division, Large Drives, Vogleweiherstr. 1-15, 90441, Nuremberg, Germany (Benjamin.eichinger@siemens.com)

Stefan Kulig; TU Dortmund University, Institute of Electrical Drives and Mechatronics; Emil-Figge-Str. 70; 44227 Dortmund (stefan.kulig@tu-dortmund.de)

Bernd Ponick; Leibniz Universität Hannover, Institute for Drive Systems and Power Electronics; Welfengarten 1; 30167 Hanover, Germany (Ponick@ial.uni-hannover.de)

Ulrich Werner; Siemens AG, Industry Sector, Drive Technologies Division, Large Drives, Vogleweiherstr. 1-15, 90441, Nuremberg, Germany (werner.ulrich@siemens.com)

II. FEM IN NOISE CALCULATION - THE ROUTE FROM EXCITATION TO VIBRATION AND NOISE

A. Electromagnetic Calculations to Determine the Force Waves

The transient electromagnetic forces have first been calculated sing a 2D model at rated and at no-load operation taking into account the non-linearities. Also inverter currents have been fed. To do this it is necessary to build up a very detailed model. Further, the mesh has to be well designed to precisely calculate the flux density B. The very fine time step of 5 µs has to be observed, and at the same time the computational effort has to be kept in mind.

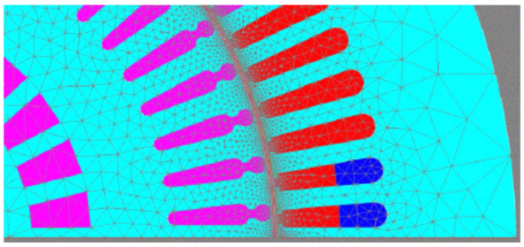

Fig. 1: Electromagnetic model to calculate the force waves up to 10 kHz

The model that was used is shown in Fig. 1. This includes nearly fifty thousand nodes, and as can be seen in the diagram, the air gap has a very fine mesh.

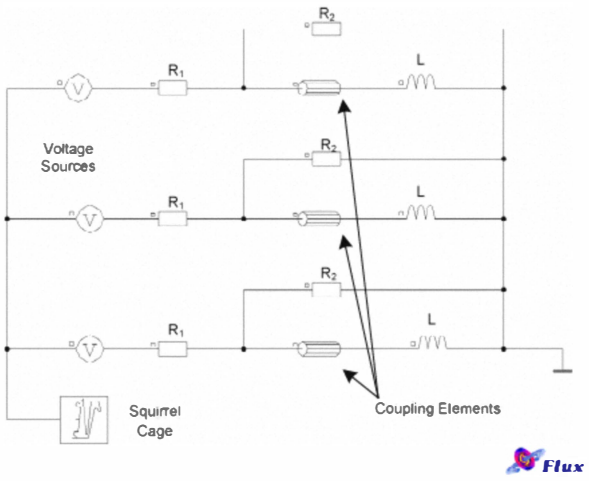

Fig. 2: Coupling circuit to inject any voltage curve

In addition to these considerations, to feed the inverter outputs, a network has been built up as shown in Fig. 2. Alternatively, current sources can be used. The resistance of each phase can be specified in the coupling elements. The series-connected inductances include the end winding inductance. Resistances *R* are just elements to simplify the post processing.

The calculations result in a matrix of the radial component of the flux density B_{rad} in the middle of the air gap. Each row contains the transient curve for each point on the circumference. In principle, it is possible to extract the tangential component of the flux density, but induction motors with a very small air gap, usually have a component B_{tan} less than 10 % of the radial component. As a consequence, the field is almost purely radial. This simplification is also made in analytical approaches.

Using the two-dimensional Fourier transformation, the curves can be transferred into separate rotating force waves [2]. These are described by a frequency, spatial harmonic number on the circumference, amplitude, phase angle and rotation direction. On one hand, these waves form the basis to make a comparison between the different calculations. On the other hand, the causes of certain vibrations can be identified more easily.

Before showing some results of the electromagnetic calculations, some elements of the theory of higher harmonics using [1] and [4] is considered to show the expected induction waves.

The first group comprises the waves caused by the stator. They are described by the harmonic number

$$\nu_1 = p \cdot (6k_1 + 1), \text{ whereas } k_1 \in Z \tag{1}$$

In this formula, p is the number of pole pairs of the fundamental wave, which is considered separately. The most pronounced waves are those that also contain the slot harmonics. With the stator slot number $N_1 = 72$, those waves have the harmonic numbers 70, 74, 142, 146 and so on. All these waves have the frequency 50 Hz. In addition to these, the saturation causes a 3rd and 5th harmonic with 150 Hz and 250 Hz.

The waves resulting from the calculations with amplitudes greater than 1 % of the fundamental are shown in Table I for the comparison of rated and no-load operation. It can be seen, that the determined induction waves can be verified by the theory and match the expected waves. Further, in no-load operation, the amplitudes of the induction waves decrease by almost 50 %. In addition to these, there are waves that are caused by the rotor. The harmonic numbers are described by

$$\nu_2 = p + k_2 N_2, \text{ where } k_2 \in Z \setminus \{0\} \tag{2}$$

and the frequency is given by

$$f_{\nu_2} = \left[1 + \left(\frac{\nu_2}{p} - 1\right) \cdot (1 - s)\right] \cdot f_1 . \tag{3}$$

In this equation s is the slip, N_2 is the rotor slot number and f_1 the frequency of the input current. Also, the higher harmonics caused by the rotor are the residual rotor fields. These result by all induction of stator waves in the rotor. The harmonic number is given by

$$\nu_2 = \nu_1 + k_2 N_2, \text{ where } k_2 \in Z \setminus \{0\} \tag{4}$$

and the frequency dependent on this by

$$f_{\nu_2} = f_{\nu_1} + \frac{k_2 N_2}{p} \cdot (1 - s) \cdot f_1 . \tag{5}$$

TABLE I
INDUCTION AIR GAP WAVES CAUSED BY THE STATOR USING SINUSOIDAL VOLTAGE SOURCES UNDER RATED AND NO-LOAD OPERATION. AMPLITUDES ARE GIVEN IN PERCENT BASED ON THE FUNDAMENTAL FOR RATED OPERATION

Harmonic number $\lvert\nu_1\rvert$ ( )	Frequency f(Hz)	B_{rad} rated operation	B_{rad} no-load operation	Deviation for no-load operation
2	50	100.00%	102.17%	2.17%
10	50	2.58%	1.50%	-41.78%
14	50	1.70%	0.87%	-48.89%
26	50	1.25%	0.66%	-46.88%
34	50	1.65%	0.83%	-49.62%
38	50	1.60%	0.80%	-49.97%
62	50	1.62%	0.86%	-47.10%
70	50	14.99%	12.57%	-16.15%
74	50	9.55%	7.33%	-23.21%
142	50	6.46%	6.51%	0.80%
146	50	5.01%	5.28%	5 52%
6	150	1.30%	0.74%	-43.10%
10	250	1.47%	1.19%	-19.11%

The index 1 relates to stator values and 2 relates to rotor values. Some of these main expected waves can be seen in Table II. The comparison of the two operating conditions shows the same trend as the stator waves.

TABLE II
INDUCTION AIR GAP WAVES CAUSED BY THE ROTOR USING SINUSOIDAL VOLTAGE SOURCES AT RATED AND NO-LOAD OPERATION. AMPLITUDES ARE GIVEN IN PERCENT BASED ON THE FUNDAMENTAL FOR RATED OPERATION

Harmonic number $\lvert\nu_2\rvert$ ( )	Frequency f(Hz) at rated	B_{rad} rated operation	Frequency f(Hz) at no-load	B_{rad} no-load operation	Deviation of no-load operation
46	1137	1.43%	1145	0.59%	-58.51%
22	1237	1.98%	1245	1.13%	-43.14%
50	1237	12.54%	1245	5.75%	-54.16%
62	1237	1.17%	1245	0.59%	-49.85%
18	1337	2.61%	1345	1.72%	-34.00%
42	1337	1.54%	1345	0.78%	-49.23%
54	1337	12.24%	1345	5.57%	-54.53%
58	1437	1.04%	1445	0.51%	-51.24%
102	2524	4.48%	2539	2.31%	-48.50%
106	2624	4.76%	2639	2.39%	-49.87%

The Maxwell stress tensor can be used to calculate the forces. Force density σ is calculated by simplifying the almost radial fields by

$$\sigma_{rad} = \frac{B_{rad}^2}{2\mu_0}, \tag{6}$$

whereas μ_0 is the magnetic field constant. Either all calculated induction waves – regardless of the cause – are

multiplied to give

$$\sigma_{rad} = \frac{1}{2\mu_0} \cdot \left[\sum_i \left(\hat{B}_{(i)} \cdot \cos\left(2\pi f_{(i)} t + \nu_{(i)} \cdot \phi_1 + \phi_{b,(i)} \right) \right) \right]^2 \quad (7)$$

where ϕ_1 is the position on the circumference and ϕ_b the phase shift, or the whole matrix B_{rad} is squared and the two-dimensional Fourier transformation performed on the new matrix σ_{rad}. The second choice is recommended, because in the first choice, a minimum peak height is set, so that small waves are neglected. However, even small induction waves can lead to significant force waves when they are multiplied by large ones.

B. Mechanical Calculations to Determine the Surface Vibration

To calculate the noise emission, it is necessary to determine the surface vibration. Therefore, a very detailed three-dimensional mechanical model has been built up in the finite element calculation tool ANSYS. It includes stator core, slot filling, housing and shields, which is hidden on one to allow the inside of the motor housing to be viewed.

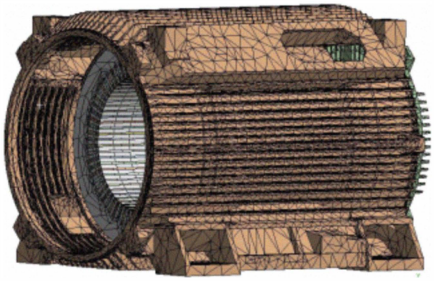

Fig. 3: Three-dimensional finite element model

To verify this, in the model shown in Fig. 3, a comparison has been made between the numerical and experimental modal analysis. [3] has treated the numerical modal analysis in detail. The experimental modal analysis has been performed for rigid and soft foundation using a shaker for penetration. The resulting vibrations have been measured at 35 points on the stator teeth and another 35 points on or between the housing ribs, as shown in Fig. 4.

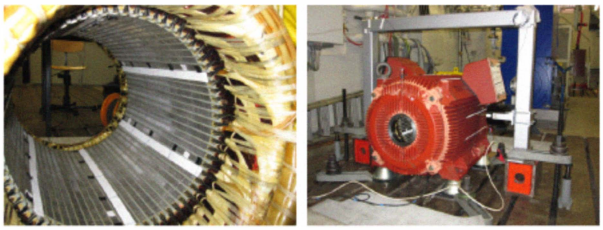

Fig. 4: Setup for the experimental modal analysis

The comparison indicates deviations of about 10 %. For the $|\nu| = 0$ modes, even less than 5 %. From this, it can be concluded that this model provides a very good match.

Harmonic solvers are mainly used in vibroacoustic applications. Based on the result, the mechanical calculations were performed in the frequency domain. Therefore, all waves with the same frequency but different spatial harmonic numbers had to be summed up complex. In addition, the force density is integrated along a tooth. This results in a force in Newton.

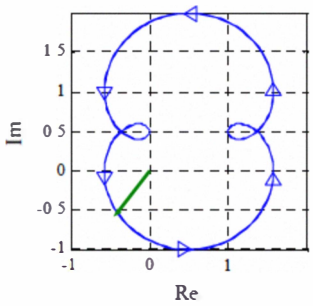

Fig. 5: The pattern along which the force vector moves seen on the circumference for the sum of $|\nu| = 4$, $|\nu| = 12$ and $|\nu = 0$ rotating force waves with different amplitudes and phase shifts

For example, to impress a $|\nu| = 4$ rotating force wave, every interpolation point along the circumference would get the same amplitude, but a different phase shift. However, if two waves are summed, then also the set amplitude would vary. The consequence is that the force vector would not move on a circle, but on a pattern which is shown as example in Fig. 5.

The surface vibration can be determined for any particular case in this way. These force waves can also be analytically calculated. The model that has been configured also provides the possibility of impressing the tangential component of the force. Its effect will be considered in future work.

C. Acoustic Calculations to Determine the Noise Emission

The third and last step is to calculate the noise emission using a 3D finite element model. To round off and verify the methods, the numerical results are being compared to measurements performed in a sound chamber.

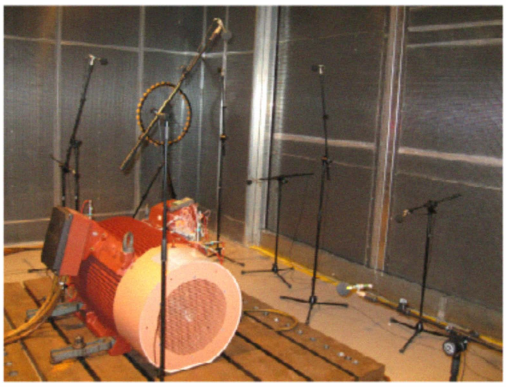

Fig. 6: Test setup in the sound chamber

The test setup is presented in Fig. 6. The measurement was performed using the enveloping surface method according to ISO 3744 with 14 microphones.

In contrast to the electromagnetic and mechanical calculations, the acoustic calculations using the acoustic finite

element calculation tool ACTRAN (ANSYS Acoustics) have been performed on three different models, which cover three frequency bands. The model to calculate the noise emission in a band from 2 kHz up to 5 kHz is shown in Fig. 7. The size of the enveloping body shown has to be the minimum of either to factor 0.5 larger than the calculated body, or the maximum wavelength being considered. Therefore, to reduce the calculation time, the frequency band has been split up into 0 – 2 kHz, 2 – 5 kHz and 5 – 10 kHz. Furthermore, the model consists of

- Coupling surface (surface of the motor)
- Finite element domain (enveloping body)
- Infinite elements on the enveloping body
- Post mesh or any points defined as microphones

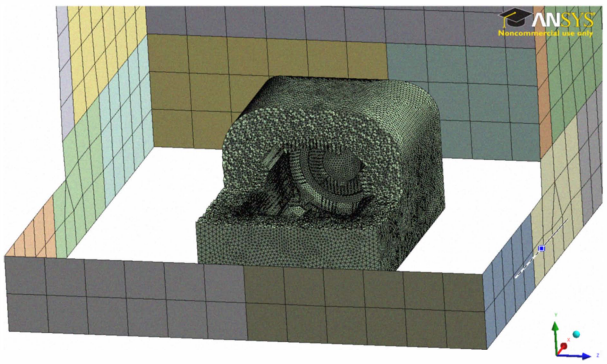

Fig. 7: Acoustic model to calculate the noise emission in a band from 2 kHz up to 5 kHz

D. Summary of the Finite Element Consideration

Summarizing, the previous sections have shown that the calculation of the noise emission is possible using the currently available software with an acceptable level of expenditure. The different meshes must be designed very well. As the acoustic considerations has shown, in some cases, it is useful to design more models to reduce the computation time. In the future, the tangential component will be considered and perhaps the possible eccentricity. Further the currently ongoing evaluation of the acoustic calculations including the comparison to the measurement will be published.

III. Embedding a Numerical Modal Matrix in an Analytical Noise Calculation

A. The Modal Theory

The mechanical structure of an electric motor can be described as a system of multiple points that are coupled with one another. Magnetic forces at points on the stator bore cause all points of the system to move. Assuming that all forces between these points are proportional with regard to mass, damping and stiffness, the motor's dynamic behavior is described by the differential equation of movement.

$$\mathbf{M}\frac{\mathrm{d}^2\vec{\xi}}{\mathrm{d}t^2}+\mathbf{D}\frac{\mathrm{d}\vec{\xi}}{\mathrm{d}t}+\mathbf{K}\vec{\xi}=\vec{F} \tag{8}$$

$\mathbf{M}$ is the mass matrix, $\mathbf{D}$ the damping matrix, $\mathbf{K}$ the stiffness matrix, $\vec{F}$ the forcing vector, $\vec{\xi}$ the response vector showing the deflection, t is time. The matrices have the dimension $n\times n$, the vectors n elements, where n is the number of points that the mechanical model of the motor consists of. This results in n degrees of freedom or rather n differential equations, which are coupled with one another. This is the reason that an analytical solution is very difficult; and even more so, as the mass, damping and stiffness between the points are unknown without making measurements or performing numerical calculations.

1) The Modal Matrix

In this case, the modal transformation offers a solution, which allows further analytical calculations based on a numerical modal analysis performed once.

When examining free oscillations ($\vec{F}=\vec{0}$) without damping, as handled in [5] by using the approach

$$\vec{\xi}=\vec{\psi}e^{j\omega_0 t} \tag{9}$$

with the eigenvector $\vec{\psi}$ and the eigenfrequency ω_0, the equation (8) changes into

$$\left(-\omega_0^2\mathbf{M}+\mathbf{K}\right)\vec{\psi}=\vec{0}. \tag{10}$$

The real eigenvalues

$$\lambda=\omega_0^2 \tag{11}$$

can be determined by calculating the non-trivial solutions from the determinant as follows:

$$\left|-\lambda\mathbf{M}+\mathbf{K}\right|=0 \tag{12}$$

The result is n eigenvalues, one for every degree of freedom.

There is one eigenvector $\vec{\psi}_{(r)}$ for every eigenvalue $\lambda_{(r)}$ with $r=1\ldots n$ satisfying the equation (10). Since every vector, which is collinear to $\vec{\psi}_{(r)}$, is a solution of the equation, the eigenvectors are scaled with the mass matrix:

$$\vec{\psi}_{(r)}^{\mathrm{T}}\mathbf{M}\vec{\psi}_{(r)}=1 \tag{13}$$

The scaled eigenvectors are written as $n\times n$ matrix and result in the modal matrix:

$$\mathbf{\Psi}=\left[\vec{\psi}_{(1)}\quad\ldots\quad\vec{\psi}_{(n)}\right] \tag{14}$$

From this definition, the correlation follows

$$\mathbf{\Psi}^{\mathrm{T}}\mathbf{K}\mathbf{\Psi}=\mathbf{\Lambda}_0=\begin{bmatrix}\omega_{0(1)}^2 & & 0\\ & \ddots & \\ 0 & & \omega_{0(n)}^2\end{bmatrix}. \tag{15}$$

At this point, it is implied, that the system matrices $\mathbf{M}$ and $\mathbf{K}$ are symmetrical.

2) Damping

In reality, there are different types of damping that appear simultaneously. When the simplified case of proportional damping is assumed, the damping matrix is a linear combination of mass and stiffness.

$$\mathbf{D} = \alpha\mathbf{M} + \beta\mathbf{K} \tag{16}$$

In this equation, α and β are scalar values.

With (13) and (15), the equation (16) converts into the modal damping matrix

$$\mathbf{\Psi}^{\mathrm{T}}\mathbf{D}\mathbf{\Psi} = \mathbf{\Psi}^{\mathrm{T}}\left(\alpha\mathbf{M} + \beta\mathbf{K}\right)\mathbf{\Psi} = \alpha\mathbf{I} + \beta\mathbf{\Lambda}_0 \tag{17}$$

I is the unity matrix. Modal decoupling is possible as $\alpha\mathbf{I} + \beta\mathbf{\Lambda}_0$ is also a diagonal matrix.

Furthermore, [6] shows, that

$$\alpha + \beta\omega_{0(r)}^2 = 2d_{(r)}\omega_{0(r)} \tag{18}$$

where $d_{(r)}$ is the damping ratio for the r^{th} oscillation mode.

3) Modal Decoupling

The operation of modal decoupling is basically a coordinate transformation. It allows the coupled system of differential equations, shown in (8), to be solved by using the modal system response vector $\vec{\Theta}$ resulting from the modal transformation.

$$\vec{\xi} = \mathbf{\Psi}\vec{\Theta} \tag{19}$$

Assuming a harmonic force excitation, it leads to a harmonic response:

$$\begin{aligned} \underline{\vec{F}} &= \underline{\hat{\vec{F}}}e^{j\omega t} \\ \underline{\vec{\Theta}} &= \underline{\hat{\vec{\Theta}}}e^{j\omega t}. \end{aligned} \tag{20}$$

Note that both the forcing and response vector can have complex amplitudes. With (19) and (20), and multiplied with the transpose modal matrix, equation (8) changes to

$$\mathbf{\Psi}^{\mathrm{T}}\left(-\omega^2\mathbf{M} + j\omega\mathbf{D} + \mathbf{K}\right)\mathbf{\Psi}\underline{\hat{\vec{\Theta}}} = \mathbf{\Psi}^{\mathrm{T}}\underline{\hat{\vec{F}}}. \tag{21}$$

Taking advantage of the orthogonality relations shown in section III.A.1), the system of differential equations is completely decoupled for each oscillation mode *r* within the modal coordinate system:

$$\left(-\omega^2 + j2d_{(r)}\omega_{0(r)}\omega + \omega_{0(r)}^2\right)\underline{\hat{\Theta}}_{(r)} = \vec{\psi}_{(r)}{}^{\mathrm{T}}\underline{\hat{\vec{F}}}. \tag{22}$$

The response for each mode conforms with

$$\underline{\hat{\Theta}}_{(r)} = \frac{\vec{\psi}^{\mathrm{T}}\underline{\hat{\vec{F}}}}{\omega_{0(r)}^2} \frac{1}{1 - \left(\dfrac{\omega}{\omega_{0(r)}}\right)^2 + j2d_{(r)}\dfrac{\omega}{\omega_{0(r)}}} \tag{23}$$

and hence gives the complex modal response vector $\underline{\hat{\vec{\Theta}}}$.

Equation (19) affords the inverse transformation to complex non-modal coordinates in order to allow the excited oscillations to be analyzed.

B. Applying the Modal Calculation

1) Model Properties

A two-dimensional mechanical model of the stator, including the winding and a housing, if existent, has to be built in a numerical finite-element program. The elements forming the model are created from a mesh of nodes. The program provides the coordinates of these nodes, the position of the first tooth, as well as the eigenfrequencies and the modal matrix for a specific number of oscillation modes, respectively modal eigenvectors. The modal values are obtained from the undamped system scaled with the mass matrix as shown in (13). A simplified view of the stator model is given in Fig. 8. In this model, ϕ_1 is the stator's coordinate angle, ϕ_t is the tooth tip width angle and R_b is the bore radius.

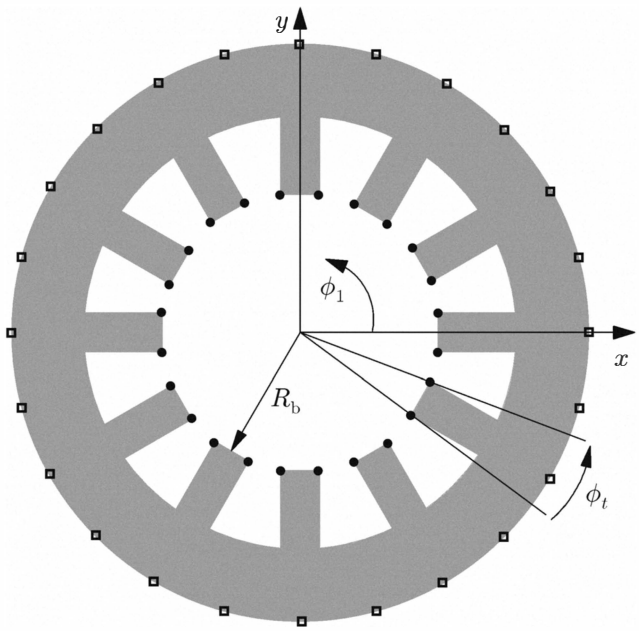

Fig. 8: Simplified view of the stator model showing relevant inner and outer nodes, as well as geometrical definitions.

With the stator's geometrical information, it is now possible to identify the two nodes per tooth at the inner tooth edges (subsequently called "inner nodes") illustrated as round dots in Fig. 8 and the nodes, which form the model's outer contour (subsequently called "outer nodes"), illustrated as square dots. Other nodes are not of interest for the further investigation.

2) Applying an Excitation Force

The spatial harmonics of the flux density $b_{(\gamma)}$ are provided by an analytical program. They are given in the form

$$\begin{aligned} b\left(\phi_1, t\right) &= \sum_i b_{(i)}\left(\phi_1, t\right) \\ &= \sum_i \hat{B}_{(i)} \cos\left(\nu_{b,(i)}\phi_1 - \omega_{b,(i)}t + \phi_{b,(i)}\right). \end{aligned} \tag{24}$$

From (24), the spatial harmonics of the radial tensile stress is calculated as used in [7] with

$$\sigma(\phi_1,t)=\left(\sum_i b_{(i)}(\phi_1,t)\right)^2\frac{1}{2\mu_0}=\sum_k \hat{\sigma}_{(k)}\cos\left(\nu_{\sigma,(k)}\phi_1-\omega_{\sigma,(k)}t+\phi_{\sigma,(k)}\right). \quad (25)$$

The tensile stress is applied to the inner nodes and translated into a force. Every inner node is subject to the stress of half a tooth tip, so the force amplitude for each node is given with

$$\hat{F}_{(k)}=\hat{\sigma}_{(k)}\frac{\phi_t}{2}lR_b \quad (26)$$

where l is the machine length.

To avoid the response amplitude being dependent on the chosen instant of time, a complex forcing vector is generated. This means that each element m of the vector representing an inner node is assigned a complex value depending on the node's coordinate angle ϕ_m and the phase angle of the exciting tensile stress harmonic.

$$\underline{\hat{F}}_{(k,m)}=\hat{F}_{(k)}e^{j\left(\nu_{\sigma,(k)}\phi_m+\phi_{\sigma,(k)}\right)} \quad (27)$$

Vector elements not representing inner nodes are set to zero.

As the generated force vector is complex, the modal response vector $\underline{\vec{\xi}}$ resulting from (23) is complex, too, especially when damping is existent. The inverse transformation (19) returns the non-modal response to the excitation, which is then analyzed along the outer nodes, in simple cases, the stator outer circumference.

3) Analyzing the Excited Surface Oscillation

Each oscillation mode is a standing wave along the motor's circumference with a dominating spatial order ν. For circular models, generally two oscillation modes exist with the same harmonic order (except zero) and frequency, but shifted through π/(2ν) with respect to one another in the stator's coordinate system. As a consequence, rotating excitations lead to rotating deformations. In the case of simple outer contours as shown in Fig. 8, the Fourier transformation of the outer node response for each excitation provides the same spatial harmonics that the deformation consists of.

When performing the Fourier transformation separately for the real and the imaginary part of the oscillation, the result is an amplitude $S_{\mathrm{re}(k,r,\rho)}$ and phase angle $\phi_{S,\mathrm{re}(k,r,\rho)}$ for the real part and accordingly for the imaginary part $S_{\mathrm{im}(\mu,r,\rho)}$ and $\phi_{S,\mathrm{im}(\mu,r,\rho)}$ for each spatial order ρ and the excitation being considered with the index k. The definite oscillation amplitudes are obtained from

$$S_{(k,r,\rho=0)}=\sqrt{\left(S_{\mathrm{re}(k,r,\rho=0)}\right)^2+\left(S_{\mathrm{im}(k,r,\rho=0)}\right)^2} \quad (28)$$

for ρ = 0 and

$$S_{(k,r,\rho)}=\left(S^2_{\mathrm{re}(k,r,\rho)}\cos^2\left(\phi_{S,\mathrm{re}(k,r,\rho)}\right)+S^2_{\mathrm{im}(k,r,\rho)}\cos^2\left(\phi_{S,\mathrm{im}(k,r,\rho)}\right)\right)^{0.5} \quad (29)$$

for ρ > 0. The dedicated phase angle is

$$\phi_{S,(k,r,\rho)}=\arctan\left(\frac{S_{\mathrm{im},(k,r,\rho)}}{S_{\mathrm{re},(k,r,\rho)}}\right) \quad (30)$$

for $S_{\mathrm{im}(k,r,\rho)}\geq 0$. Considering the correct quadrant, for $S_{\mathrm{im}(k,r,\rho)}<0$ and $S_{\mathrm{re}(k,r,\rho)}\geq 0$, it is necessary to add π to the value of the phase angle, respectively to subtract π in the case of $S_{\mathrm{im}(k,r,\rho)}<0$ and $S_{\mathrm{re}(k,r,\rho)}<0$. The oscillation frequency is

$$\omega_{S,(k,r,\rho)}=\omega_{\sigma,(k)}. \quad (31)$$

As a linear system is assumed, a superposition of all spatial harmonics of the surface deformation resulting from different excitations is permitted.

$$S=\sum_k\sum_r\sum_\rho\left(S_{(k,r,\rho)}\cdot\cos\left(\rho\phi_1-\omega_{S,(k,r,\rho)}t+\phi_{S,(k,r,\rho)}\right)\right) \quad (32)$$

4) Sound Emissions

Based on these results, acoustic emissions can be calculated from these surface oscillations. Still employing an analytical method, [8] described the calculation of sound pressure for electrical machines in the far sound field, simplifying the machine as an acoustic monopole and using a relative radiant power depending on the harmonic order and frequency of the deformation. A further development of this work is given in [8].

C. Verification

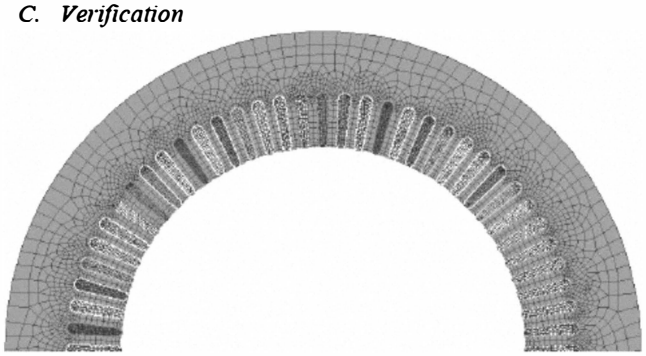

Fig. 9: Half of the analytical model that is used to calculate the modal matrix.

A two dimensional model of a motor has been created at the Technical University of Dortmund with the FEM-Software ANSYS. With this model, the data listed in section III.B.1) has been derived for the analytical analysis at the Leibniz Universität Hannover. The model features a circular outer contour. A detail is shown in Fig. 9.

Both models had been excited by the same spatial harmonic radial tensile stress. After a calculation, the surface deformation of the results form ANSYS and those of the

analytical method here presented had been analyzed via Fourier transformation and compared to each other. For the analytical method, eigenvectors with the main spatial orders $\nu = 0\ldots6$ along the motor's circumference had been included, whereas the numerical calculation is based on a different procedure. The whole system of equations is set up and solved using the method of finite elements.

The first excitation tested is

$$\sigma(\phi_1, t) = 100\text{kNm}^{-2} \cos(0 \cdot \phi_1 - 2\pi \cdot 1000\text{Hz} \cdot t).$$

The resulting amplitudes of the surface deformation are listed in TABLE III for each harmonic order. The analytical method shows a difference of 1.9 % to the amplitude, which had been calculated numerically and is hence very close to the numerically determined result.

In a second examination, the stress

$$\sigma(\phi_1, t) = 100\text{kNm}^{-2} \cos(4 \cdot \phi_1 - 2\pi \cdot 1000\text{Hz} \cdot t)$$

had been applied. As TABLE IV shows, the difference is 4.2 % and therefore almost as good as in the first comparison. It must be mentioned that the analytical calculation also results in some "noise", i.e. small amplitudes occur for spatial orders that are not excited. This "noise" is already existent in the eigenvectors and shows amplitudes, which are smaller by a factor 100…1000 than the main harmonic.

In a third test, specifically single nodes were excited by an oscillating force. The nodes of two opposed teeth were excited with 1 kN at 1 kHz each, but in phase opposition; the results are shown in TABLE V. Again there is a very good correlation.

TABLE III
COMPARISON OF NUMERICAL AND ANALYTICAL RESULTS IN SURFACE OSCILLATION AMPLITUDES FOR EXCITATION $100\text{kNm}^{-2} \cos(0 \cdot \phi_1 - 2\pi \cdot 1\text{kHz} \cdot t)$

Spatial order ρ	Numerical (ANSYS) (µm)	Analytical (µm)	Difference (%)
0	0.3096	0.3037	-1.9
1	0	0.0004	/
2	0	0.0003	/
3	0	0.0054	/
4	0	0.0027	/
5	0	0.0034	/
6	0	0.0024	/

TABLE IV
COMPARISON OF NUMERICAL AND ANALYTICAL RESULTS IN SURFACE OSCILLATION AMPLITUDES FOR EXCITATION $100\text{kNm}^{-2} \cos(4 \cdot \phi_1 - 2\pi \cdot 1\text{kHz} \cdot t)$

Spatial order ρ	Numerical (ANSYS) (µm)	Analytical (µm)	Difference (%)
0	0	0.0011	/
1	0	0.0012	/
2	0	0.0003	/
3	0	0.0024	/
4	0.3477	0.3331	-4.2
5	0	0.0004	/
6	0	0.0026	/

TABLE V
COMPARISON OF NUMERICAL AND ANALYTICAL RESULTS IN SURFACE OSCILLATION AMPLITUDES FOR EXCITATION AT TWO OPPOSED TEETH (1 KN, 1 KHZ)

Spatial order ρ	Numerical (ANSYS) (µm)	Analytical (µm)	Difference (%)
0	0.0156	0.0150	-3.9
1	0	0.0012	/
2	8.6835	8.7823	+1.1
3	0	0.0024	/
4	0.0333	0.0309	-7.2
5	0	0.0004	/
6	0.0068	0.0065	-4.4

When considering the fact that the numerical calculation had taken about 100 to 1000 times longer than the analytical method, it can be concluded that the analytical method provides a significant benefit in the practical use. This advantage is even higher when examining three-dimensional models.

Of course a numerical model has to be generated once to obtain the modal matrix. But after that it is possible to very quickly calculate the surface oscillation and noise emission for numerous different operation points, electrical values, variations of the winding and even different rotors, as long as the stator's mechanical attributes do not change.

The results of conventional, pure analytical calculations of surface oscillations are subject to several simplifications in the motor's geometry and therefore feature a lower accuracy. In contrast, the analytical noise calculation with an embedded numerically obtained modal matrix offers a high accuracy, compared to the numerical results, as shown. The mechanical complexity is only dependant on the numerical model. That means that it is possible to consider any type of slot form, outer contour and housing.

IV. CONCLUSIONS

The methods that have been discussed offer two possible basic applications:

The modal matrix as part of the analytical noise calculation shows more precise information about the acoustic quality of a customized electrical design. The complex geometries of motor housings no longer have to be simplified by a ring. Once the modal matrix is calculated using the finite element method, the change of noise radiation for any electrical customized design can be calculated very quickly.

For advanced development, the calculation of the electromagnetic radial force wave and the noise radiation using finite element method leads to more accurate results. The depicted method enables a new way to estimate the electromagnetically excited noise and will lead to a faster optimization process and less prototype measurements.

V. REFERENCES

[1] G. Müller, and B. Ponick, *Theorie of Electrical Machines, (Theorie elektrischer Maschinen),* WileyVCH, 2009.

[2] R. Hoffmann, *Bases of Frequency Analysis,* (*Grundlagen der Frequenzanalyse)*, Expert Verlag, 2001.

[3] M. Al Nahlaoui, *Natural Frequencies and Vibration Behavior of an Asynchronous Machine, (Eigenfrequenzen und Schwingungsverhalten einer Asynchronmaschine),* TU Dortmund University, 2008.

[4] H. O. Seinsch, *Higher Harmonic Phenomena of Rotary Field Machines,* (*Oberfeld Erscheinungen in Drehfeldmaschinen),* B.G. Teubner Stuttgart, 1992.

[5] H. G. Natke, *Introduction in theory and practice of time series and modal analysis,* (*Einführung in Theorie und Praxis der Zeitreihen- und Modalanalyse),* Wiesbaden, Braunschweig: Vieweg, 1983, ch. 5.

[6] P. Eibelshäuser, *Computer-aided experimental modal analysis via stepped sine wave excitation,* (*Rechnergestützte experimentelle Modalanalyse mittels gestufter Sinusanregung).* Berlin, Heidelberg, New York, London, Paris, Tokyo Hongkong: Springer-Verlag, 1990, ch. 1.

[7] H. Tappel, *About the noise of rotating field machines,* (*Über die Geräusche von Drehfeldmaschinen),* Dissertation at the University of federal armed forces Hamburg, 1992

[8] Z. Üner, *About the determination of the magnetic noise sound level of synchronous machines*, (*Über die Ermittlung der Lautstärke des magnetischen Lärms von Drehstromasynchronmotoren mit Käfigläufer),* Dissertation at the Technical University of Hanover, 1964

[9] R. Hoffmann, H. Jordan, M. Weis, *Equivalent Emitter for determination of the sound power of rotating machines,* (*Ersatzstrahler zur Ermittlung der Schalleistung von rotierenden Maschinen)*, Journal for noise control. (Zeitschrift für Lärmbekämpfung), 1966

[10] M. Al Nahlaoui, S. Kulig, U. Werner, *Electromechanical Forces and Vibration of an Asynchronous Machine for Sinusoidal and Inverter Currents,* 12th Portuguese-Spanish Conference on Electrical Engineering, 2011

M. Al Nahlaoui was born in Bremerhaven, Germany, in January 1985. In 2008, he received the Dipl.-Ing. degree in electrical engineering from the TU Dortmund University in Dortmund.
He has been with the TU Dortmund University, Institute of Electrical Drives and Mechatronics since 2006 as student assistant and since 2008 as scientific employee. His scientific interests include finite element modeling in electromagnetic, mechanical and acoustic applications.

D. Braunisch was born in Bremen, Germany, in April 1980. In 2007 he received the Dipl.-Ing. degree in electrical engineering from the Leibniz Universität Hannover, Hanover, Germany.
He has been with the Institute of Drive Systems and Power Electronics at the University of Hanover since 2005 as student assistant and since 2007 as scientific employee. He wrote his diploma thesis at the same institute in 2007. His scientific interests include electromagnetically excited noise in electrical machines, analytical and numerical magnetic field calculation.

B. Eichinger was born in Erlangen, Germany, in December 1980. In 2005 he received the Dipl.-Eng. (FH) degree in mechanical engineering from the University of Applied Sciences in Nuremberg.
He has been with Siemens AG, Industry Sector, Drive Technologies Division, Large Drives, Nuremberg, Germany since 2005. While working for Siemens he received the M. Eng. degree from the University of Applied Sciences in Nuremberg in 2007. His scientific interests include technical acoustics, mechanics and strength of materials.

T. Stefan Kulig was born in Krakow, Poland. He graduated from the Technical University Krakow as a Master of Science in Heavy Electrical Engineering. In recognition of his in-depth investigation of the inner asymmetry of electrical machines, the Krakow Technical University conferred on him the degree of Doctor of Engineering in 1974. He moved to Western Germany in 1971 and joined the Generator Development Department of Kraftwerk Union AG (now Siemens Westinghouse) in Mülheim/Ruhr. His work has concentrated on the analysis of dynamics of large turbo generators. In particular, he has been involved in the investigation of electro-mechanical transients in turbine-generators arising from electrical disturbances. At last he worked as departmental conductor in senior management. In recognition of recent research into phase-and-winding-short circuits in turbo generators he was in 1979 awarded a second doctorate by the University of Hannover, Germany. In 1987 he received the venia legendi for "Electrical Machines and Drives" and qualified as a professor at the Fern-University Hagen. He has held the chair of Electrical Drives and Mechatronics at the Technical University of Dortmund since 1996.

B. Ponick received the Dipl.-Ing. degree in 1990 and the Dr.-Ing. (Ph.D.) degree in 1994, both from Leibniz Universität Hannover (LUH) , Hanover, Germany. From 1995 to 2003, he was with Siemens AG, Dynamowerk Berlin, Germany, where he started as a design engineer for large variable speed motors and later became head of the electrical design department and finally technical director of Siemens Dynamowerk. In 2003, he became a Full Professor for Electrical Machines and Drive Systems at the Leibniz Universität Hannover. His research interests include design and prediction methods for electrical machines, important parasitic effects like magnetic noise, torque pulsations or bearing currents, energy efficient motors, electric motors for road vehicles and micro acutators. Since 2007, Prof. Ponick is chairman of IEC TC2 'Rotating Machinery' and thus responsible for the international standardization of rotating electrical machines. In addition, he serves as academic dean for electrical engineering and information technology, managing director of the Hanover Center for Mechatronics (MZH) and member of the board of the Automotive Research Center of Lower Saxony (NFF).

Ulrich Werner was born in Erlangen, Germany, in February 1969. He received the Dipl.-Ing. degree from the University of Erlangen-Nuremberg, Germany in 1994. In 2006, he received the Dr.-Ing. degree from the University of Darmstadt, Germany.
He has been working for Siemens AG, Industry Sector, Drive Technologies Division, Large Drives, Nuremberg, Germany since 1994. His scientific interests include simulation of machine vibrations, rotor dynamics, especially for electrical machines. Dr. Werner is member of the VDI and VDE.